Heat Mass Transfer (2007) 43:965–974
DOI 10.1007/s00231-006-0171-1

ORIGINAL

Exact analytical solutions for thermosolutal Marangoni convection in the presence of heat and mass generation or consumption

Eugen Magyari · Ali J. Chamkha

Received: 11 April 2006 / Accepted: 8 June 2006 / Published online: 1 August 2006

Abstract The steady laminar thermosolutal Marangoni convection in the presence of temperature-dependent volumetric heat sources/sinks as well as of a first-order chemical reaction is considered in this paper. Assuming that the surface tension varies linearly with temperature and concentration and that the interface temperature and concentration are quadratic functions of the interface arc length x, exact analytical similarity solutions are obtained for the velocity, temperature and concentration fields. The features of these exact solutions as functions of the physical parameters of the problem are discussed in detail.

List of symbols

b	parameter, Eq. 31a
c	dimensional concentration, Eq. 4
c_p	specific heat at constant pressure, Eq. 3
C	dimensionaless concentration, Eq. 8
C_0	dimensional constant, Eq. 7b
D	mass diffusivity, Eq. 4
f_0	normal component of the dimensionless interface velocity, Eq. 13
$f'(0)$	tangential component of the dimensionless interface velocity
$f(\eta)$	similar stream function
K	dimensionless chemical reaction coefficient
L	reference length, Eq. 14
$\dot{m}$	mass flow rate per unit span, Eq. 16
M	confluent hypergeometric function, Eqs. 34
Pr	Prandtl number, $Pr = \nu/\alpha$
Q_0	dimensional heat generation/absorption coefficient, Eq. 3
r	ratio of the solutal and thermal Marangoni numbers, Eq. 13
R	positive, dimensionl chemical reaction parameter, Eq. 4
$\bar{R}$	Parameter, Eq. 24
$s_{1,2}$	parameters, Eq. 24
Sc	Schmidt number, $Sc = \nu/D$
T	temperature
T_0	dimensional constant, Eq. 7b
u,v	x- and y-component of the dimensional velocity, respectively
v_0	normal component of the dimensional interface velocity, Eq. 7b
w	dependent variable, Eqs. 31
z	independent variable, Eqs. 31
x,y	Cartesian coordinates

Greek symbols

α	thermal diffusivity, Eq. 3
Δ	discriminant, Eq. 25
γ	coefficients, Eq. 5
η	similarity independent variable, Eq. 8
ϕ	dimensionless heat generation/absorption coefficient, Eq. 13
μ	dynamic viscosity
υ	kinematic viscosity, $\nu = \mu/\rho$

E. Magyari (✉)
Institute of Building Technology, ETH Zürich,
Wolfgang-Pauli-Str.1, 8093 Zurich, Switzerland
e-mail: magyari@hbt.arch.ethz.ch

A. J. Chamkha
Manufacturing Engineering Department,
The Public Authority for Applied Education and Training,
P. O. Box 42325, Shuweikh 70654, Kuwait

θ temperature similarity variable, Eq. 8
ρ density
σ surface tension, Eq. 5
ψ stream function, Eq. 8

Subscripts
T thermal quantity
c solutal quantity
0 at $\eta = 0$
∞ for $\eta \to \infty$

1 Introduction

Marangoni boundary layers are dissipative layers which may occur along the liquid–liquid or liquid–gas interfaces. The surface tension gradients that are responsible for Marangoni convection can be both temperature and/or concentration gradients. The basic research work in this field has first been promoted by Napolitano [1, 2]. Marangoni flow induced by surface tension variations along the liquid–fluid interface causes undesirable effects in crystal growth melts in the same manner as buoyancy-induced natural convection [3, 4]. These undesirable effects become even dominant in the absence of buoyancy forces in the microgravity environment of space-based crystal growth experiments [4, 5].

In spite of its significance and relevance in microgravity crystal growth, welding, semiconductor processing and several other fields of space science, thermosolutal Marangoni convection has not been fully explored especially regarding preliminary questions of general and basic nature. As being pointed out by Napolitano [6], for classical (i.e. non-Marangoni layers) boundary layers, the field equations in the bulk fluids do not depend explicitly on the geometry of the interface when using as coordinates the arc length (x), and that the distance normal to the interface involves the mean curvature of its hydrostatic and dynamic shapes. This, together with the other surface balance equations, introduces kinematic, thermal and pressure couplings for the flow fields in the two fluids. Napolitano and Golia [7] have shown that the fields are uncoupled when the momentum and energy resistivity ratios of the two layers and the viscosity ratio of the two fluids are much less than one. Furthermore, as shown by Napolitano and Russo [8], similarity solutions for Marangoni boundary layers exist when the interface temperature gradient varies as a power of the interface arc length (x). The power laws for all other variables, including the mean curvature, were determined. Numerical solutions were found, analyzed and discussed on Marangoni boundary layers in subsequent papers by Golia and Viviani [9, 10], Napolitano et al. [11] and Pop et al. [12].

The numerous investigations of Marangoni flow in various geometries have been reviewed in the literature [13, 14]. Some of the papers most relevant to this work include the order-of-magnitude analysis of Marangoni flow given by Okano et al. [15] that gave the general trends for the variation of the Reynolds number with the Grashof number, Marangoni number, and Prandtl number. Hirata and his co-workers experimentally and numerically investigated Marangoni flow for various substances in geometries with flat surfaces relevant to this work [13, 15, 16]. Arafune and Hirata [17] presented a similarity analysis for just the velocity profile for Marangoni flow that is very similar to this derivation but the results are effectively limited to surface tension variations that are linearly related to the surface position. Slavtchev and Miladinova [18] presented similarity solutions for surface tension that varied as a quadratic function of the temperature as would occur near a minimum. Schwabe and Metzager [19] experimentally investigated Marangoni flow on a flat surface combined with natural convection in a unique geometry where the Marangoni effect and the buoyancy effect could be varied independently. Christopher and Wang [3] studied Prandtl number effects for Marangoni convection over a flat surface and presented approximate analytical solutions for the temperature profile for small and large Prandtl numbers.

Napolitano et al. [20] considered double-diffusive boundary layer along a vertical free surface. Pop et al. [12] analyzed thermosolutal Marangoni forced convection boundary layers that can be formed along the surface, which separates two immiscible fluids in surface driven flows when the Reynolds number is large enough. They derived similarity equations for the case in which an external pressure gradient is imposed and produced numerical results for these equations based on the Keller-box and superposition methods. Recently, Al-Mudhaf and Chamkha [21] reported numerical and approximate results for thermosolutal Marangoni convection along a permeable surface in the presence of heat generation or absorption and a first-order chemical reaction effects. As mentioned by Christopher and Wang [3], for an interface with evaporation or condensation at the surface, the temperature distribution along the interface is primarily a function of the vapor temperature and the heat transfer

coefficient rather than the Marangoni flow. For instance, Christopher and Wang [22] showed that the calculated temperature distribution in vapor bubble attached to a surface and in the liquid surrounding the bubble was primarily due to the heat transfer through the vapor rather than in the liquid region and the temperature variation along the surface was not linear but could be described by a power-law function. For this reason, it is assumed that both the wall temperature and solute concentration are power-law functions of the distance along the plate surface.

In none of the above references, exact analytical solutions of Marangoni flows were attempted. This is due to the inherent complexity of such flows. The present work considers thermosolutal Marangoni convective flow over a liquid–fluid interface due to imposed temperature and concentration gradients. The analysis assumes that the surface tension varies linearly with temperature and concentration but the wall temperature and concentration variations are quadratic functions of the location. A temperature-dependent heat source or sink as well as a first-order chemical reaction are assumed to exist. The main purpose of this work is to report exact analytical solutions for the stream function, velocity, temperature and solute concentration fields and to study the effect of parameters on the existence of solutions.

2 Governing equations and problem formulation

Consider steady laminar themosolutal Marangoni boundary layer flow of a viscous Newtonian fluid in the presence of heat and mass generation or consumption. The mass consumption is modeled by a first-order chemical reaction that may exist between the two fluids. The interface temperature and concentration are assumed to be quadratic functions of the distance x along the intersurface. Unlike the Boussineq effect on the body force term in buoyancy-induced flows, the Marangoni surface tension effect acts as a boundary condition on the governing equations of the flow field. The governing equations for this investigation are based on the balance laws of mass, linear momentum, energy and concentration species. Taking the above assumptions into consideration, these equations can be written in dimensional form as

$$\frac{\partial u}{\partial x}+\frac{\partial v}{\partial y}=0 \tag{1}$$

$$u\frac{\partial u}{\partial x}+v\frac{\partial u}{\partial y}=\upsilon\frac{\partial^2 u}{\partial y^2} \tag{2}$$

$$u\frac{\partial T}{\partial x}+v\frac{\partial T}{\partial y}=\alpha\frac{\partial^2 T}{\partial y^2}+\frac{Q_0}{\rho c_p}(T-T_\infty) \tag{3}$$

$$u\frac{\partial c}{\partial x}+v\frac{\partial c}{\partial y}=D\frac{\partial^2 c}{\partial y^2}-R(c-c_\infty) \tag{4}$$

The surface tension is assumed to depend on temperature and concentration linearly,

$$\sigma=\sigma_0[1-\gamma_{\mathrm{T}}(T-T_\infty)-\gamma_{\mathrm{c}}(c-c_\infty)] \tag{5}$$

where

$$\gamma_{\mathrm{T}}=-\frac{1}{\sigma_0}\frac{\partial\sigma}{\partial T}\bigg|_{\mathrm{c}},\quad \gamma_{\mathrm{c}}=-\frac{1}{\sigma_0}\frac{\partial\sigma}{\partial c}\bigg|_{\mathrm{T}} \tag{6}$$

denote the temperature and concentration coefficients of the surface tension, respectively.

The boundary conditions of this problem are given by

$$\mu\frac{\partial u}{\partial y}\bigg|_{y=0}=-\frac{\partial\sigma}{\partial x}\bigg|_{y=0}=\sigma_0\left(\gamma_{\mathrm{T}}\frac{\partial T}{\partial x}\bigg|_{y=0}+\gamma_{\mathrm{c}}\frac{\partial c}{\partial x}\bigg|_{y=0}\right) \tag{7a}$$

$$\begin{aligned} &v(x,0)=v_0,\quad T(x,0)=T_\infty+T_0X^2,\\ &c(x,0)=c_\infty+C_0X^2,\quad X=x/L \end{aligned} \tag{7b}$$

$$u(x,\infty)=0,\quad T(x,\infty)=T_\infty,\quad c(x,\infty)=c_\infty \tag{7c}$$

where L is a reference length (which will be specified below) and T_0 and C_0 are (positive or negative) dimensional constants. The coordinate system, the velocity components and the interface condition are shown in Fig. 1.

Introducing the stream function ψ (x,y) by the usual definition $u = \partial\psi/\partial y$, $v = -\partial\psi/\partial x$ as well as the similarity transformations

$$\begin{aligned} \psi(x,y)&=\upsilon X f(\eta),\\ \eta&=y/L\\ T(x,y)&=T_\infty+T_0X^2\theta(\eta)\\ c(x,y)&=c_\infty+C_0X^2C(\eta) \end{aligned} \tag{8}$$

the boundary value problem, Eqs. 1–7, reduces to the solution of the ordinary differential equations

$$f'''+ff''-f'^2=0 \tag{9}$$

$$\frac{\theta''}{Pr}+f\theta'+(\phi-2f')\theta=0 \tag{10}$$

$$\frac{C''}{Sc}+f\,C'-(K+2f')C=0 \tag{11}$$

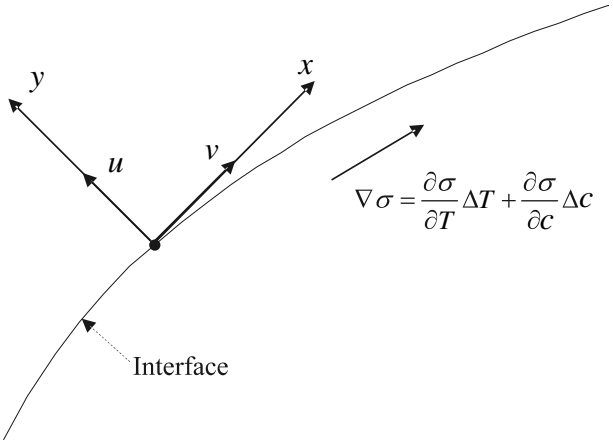

Fig. 1 Physical model, coordinate system and interface condition

along with the boundary conditions

$$f(0) = f_0, \quad f''(0) = -2(1+r), \quad \theta(0) = 1, \quad C(0) = 1,$$
$$f'(\infty) = 0, \quad \theta(\infty) = 0, \quad C(\infty) = 0. \tag{12}$$

In the above equations $Pr = \upsilon/\alpha$ and $Sc = \upsilon/D$ denote the Prandtl and the Schmidt numbers, respectively and ϕ, K, f_0 and r are further dimensionless parameters defined as follows:

$$\phi = \frac{Q_0 L^2}{\rho \upsilon c_p}, \quad K = \frac{RL^2}{\upsilon}, \quad f_0 = f(0) = -\frac{v_0 L}{\upsilon},$$
$$r = \frac{C_0 \gamma_c}{T_0 \gamma_T} \tag{13}$$

The reference length L has been chosen as

$$L = -\frac{\mu\upsilon}{\sigma_0 T_0 \gamma_T} \tag{14}$$

Having in view that with increasing temperature the surface tension σ in general decreases, its temperature gradient γ_T given by Eq. 6 is positive. Thus, the reference length chosen according to Eq. 14 is positive only if T_0 is negative. We also mention that the parameter r represents precisely the ratio of the solutal and thermal Marangoni numbers $Ma_c = \sigma_0 \gamma_c C_0 L/(\alpha\mu)$ and $Ma_T = \sigma_0 \gamma_T T_0 L/(\alpha\mu)$, respectively.

Equations 9–12 show that the f-boundary value problem is decoupled from the temperature and concentration boundary value problems. Its solution $f = f(\eta)$ (see Sect. 3) yields the dimensional velocity field in the form

$$u(x,y) = \frac{\upsilon}{L} X f'(\eta), \quad v(x,y) = -\frac{\upsilon}{L} f(\eta) \tag{15}$$

The local mass flow in the boundary layer per unit span is given by :

$$\dot{m} = \rho \int_0^\infty u \, dy = \rho\upsilon[f(\infty) - f_0]X \tag{16}$$

where $f(\infty)$ represents the similar entrainment velocity, $f(\infty) = -(L/\upsilon)v(x,\infty)$. In this way we obtain

$$\dot{m} = \rho x[v(x,0) - v(x,\infty)] \tag{17}$$

The boundary value problem, Eqs. 9–12, has been investigated numerically for different values of the parameters involved by Al-Mudhaf and Chamkha [21]. An approximate analytical solution has also been given in [21]. As already mentioned, the aim of the present paper is (a) to show that the problem 9–12 admits exact analytical solutions for all three dimensionless function $f(\eta)$, $\theta(\eta)$ and $C(\eta)$, and (b) to discuss the features of these solutions in terms of the parameters Pr, Sc, ϕ, K, f_0 and r in some detail.

3 Exact solutions of the flow problem

The momentum boundary value problem is specified by equation

$$f''' + ff'' - f'^2 = 0 \tag{18}$$

and the boundary conditions

$$f(0) = f_0, \quad f''(0) = -2(1+r), \quad f'(\infty) = 0 \tag{19}$$

The function

$$f(\eta) = f_\infty + (f_0 - f_\infty)e^{-f_\infty \eta} \tag{20}$$

is an exact solution of Eq. 18 for any value of the similar entrainment velocity $f_\infty = f(\infty)$. The asymptotic condition $f'(\infty) = 0$ requires $f_\infty > 0$. The boundary condition $f(0) = f_0$ is satisfied automatically, and the boundary condition $f''(0) = -2(1 + r)$ implies

$$f_\infty^3 - f_0 f_\infty^2 - 2(1+r) = 0 \tag{21}$$

i.e., for given values of the parameters f_0 and r, f_∞ must be a non-negative root of the cubic equation 21. Then, the similar surface velocity is obtained as

$$f'(0) = f_\infty(f_\infty - f_0) \tag{22}$$

The three roots of Eq. 21 can be calculated exactly from Cardano's equations

$$f_\infty^{(1)} = \frac{f_0}{3} + s_1 + s_2 \tag{23a}$$

$$f_\infty^{(2)} = \frac{f_0}{3} - \frac{s_1 + s_2}{2} + \frac{i\sqrt{3}}{2}(s_1 - s_2) \tag{23b}$$

$$f_\infty^{(3)} = \frac{f_0}{3} - \frac{s_1 + s_2}{2} - \frac{i\sqrt{3}}{2}(s_1 - s_2) \tag{23c}$$

where

$$s_1 = \sqrt[3]{\bar{R} + \sqrt{\Delta}}, \tag{24a}$$

$$s_2 = \sqrt[3]{\bar{R} - \sqrt{\Delta}}, \tag{24b}$$

$$\bar{R} = 1 + r + \left(\frac{f_0}{3}\right)^3 \tag{24c}$$

and

$$\Delta = 2(1+r)\left[\left(\frac{f_0}{3}\right)^3 + \frac{1+r}{2}\right] \tag{25}$$

The discriminant Δ becomes zero for $r = -1$ independent of the value of f_0, as well as for $r \neq -1$ when

$$f_0 = -3\left(\frac{1+r}{2}\right)^{1/3} \quad (\Delta = 0) \tag{26}$$

The general features of the roots $\left\{f_{\infty,}^{(1)} f_{\infty,}^{(2)} f_\infty^{(3)}\right\}$ as functions of the parameters f_0 and r, as well as their expressions for $\Delta = 0$ are summarized in Table 1 and in Fig. 2. It is worth emphasizing here that for $r = -1$ and $f_0 \geq 0$ the roots of Eq. 21 have a special meaning (see the middle row of Table 1). Indeed, in this case we have $f_\infty = f_0 \geq 0$ which implies $f(\eta) = \text{const.} = f_\infty = f_0 \geq 0$.

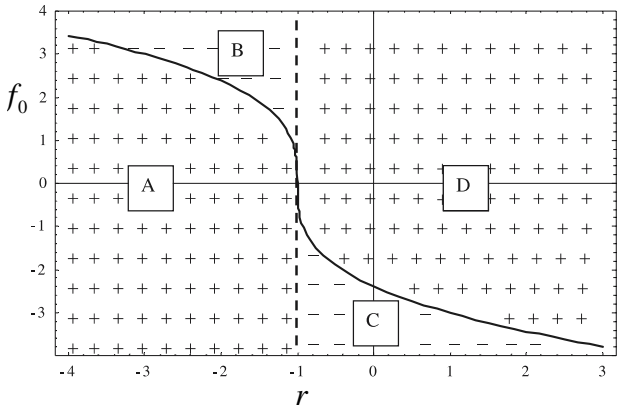

Fig. 2 The solid curve is the plot of Eq. 26 for which the discriminant Δ vanishes when $r \neq -1$. The dashed vertical line corresponds to $r = -1$ (for which the discriminant is identically zero). The signs + and − are the signs of the Δ in the domains A, B, C and D of the parameter plane (r, f_0). In the domain A no physical (i.e. real and non-negative) roots of the cubic equation 21 exist. In the domains C and D, as well as on the lower branch of the solid $\Delta = 0$-curve, a single physical root is possible, while in the domain B two physical solutions exist which on the upper branch of the solid $\Delta = 0$-curve become coincident (see also Table 1)

Hence the case $f(\eta) = f_\infty = f_0 = 0$ corresponds to the equilibrium state of the fluids. In the case $f(\eta) = f_\infty = f_0 > 0$, on the other hand, only the tangential velocity component u is vanishing while the normal velocity component v is a non-vanishing constant, $v = \upsilon f_0/L$.

Some of the basic features of the roots $\left\{f_{\infty,}^{(1)} f_{\infty,}^{(2)} f_\infty^{(3)}\right\}$ summarized in Table 1, can be extracted easily from the sign of Δ and from their relationships to the coefficients of the cubic equation 21 given by

$$f_\infty^{(1)} + f_\infty^{(2)} + f_\infty^{(3)} = f_0 \tag{27a}$$

Table 1 Features of the roots of the cubic equation 21 as functions of the parameters f_0 and r

	$f_0 < -3\left(\frac{1+r}{2}\right)^{1/3}$	$f_0 = -3\left(\frac{1+r}{2}\right)^{1/3}$ (the solid curve of Fig. 1)	$f_0 > -3\left(\frac{1+r}{2}\right)^{1/3}$
$r < -1$	$f_\infty^{(\mathrm{I})} < 0$, $f_\infty^{(\mathrm{II})}, f_\infty^{(\mathrm{III})}$ = complex conjugate. $\Delta > 0$ Domain A	$f_\infty^{(I)} = \left(\frac{1+r}{2}\right)^{1/3} < 0$, $f_\infty^{(\mathrm{II})} = f_\infty^{(\mathrm{III})} = -2\left(\frac{1+r}{2}\right)^{1/3} > 0$ $\Delta = 0$ (upper branch)	$f_\infty^{(\mathrm{I})} < 0$ $f_\infty^{(\mathrm{II})}, f_\infty^{(\mathrm{III})} > 0$ $\Delta < 0$ Domain B
$r = -1$ (the dashed vertical line of Fig. 1)	$f_\infty^{(\mathrm{I})} = f_0 < 0$ $f^{(\mathrm{II})}{}_\infty = f^{(\mathrm{III})}{}_\infty = 0$, $\Delta = 0$	$f_\infty^{(1)} = f_\infty^{(2)} = f_\infty^{(3)} = 0$ $\Delta = 0$	$f_\infty^{(\mathrm{I})} = f_0 > 0$ $f_\infty^{(\mathrm{II})} = f_\infty^{(\mathrm{III})} = 0$, $\Delta = 0$
$r > -1$	$f_\infty^{(\mathrm{I})} > 0$ $f_\infty^{(\mathrm{II})}, f_\infty^{(\mathrm{III})} < 0$ $\Delta < 0$ Domain C	$f_\infty^{(I)} = \left(\frac{1+r}{2}\right)^{1/3} > 0$, $f_\infty^{(\mathrm{II})} = f_\infty^{(\mathrm{III})} = -\left(\frac{1+r}{2}\right)^{1/3} < 0$ $\Delta = 0$ (lower branch)	$f_\infty^{(\mathrm{I})} > 0$, $f_\infty^{(\mathrm{II})}, f_\infty^{(\mathrm{III})}$ = complex conjugate $\Delta > 0$ Domain D

Here $\left\{f_{\infty,}^{(I)} f_{\infty,}^{(II)} f_\infty^{(III)}\right\}$ is some sequence of the roots (23a, b, c). Only the non-negative roots are physical. The solid curve, the dashed vertical line (both associated with $\Delta = 0$) as well as domains A, B, C and D of the parameter plane (r, f_0) are shown in Fig. 2

$$f_\infty^{(1)} f_\infty^{(2)} + f_\infty^{(1)} f_\infty^{(3)} + f_\infty^{(2)} f_\infty^{(3)} = 0 \tag{27b}$$

$$f_\infty^{(1)} f_\infty^{(2)} f_\infty^{(3)} = 2(1+r) \tag{27c}$$

Indeed, Eq. 27b shows that it is not possible that all three roots $\left\{f_{\infty,}^{(1)} f_{\infty,}^{(2)} f_\infty^{(3)}\right\}$ are simultaneously positive or simultaneously negative. Therefore, we can obtain at most dual exact solutions (but never triple solutions) for given values of the input parameters f_0 and r. Furthermore, Eq. 27c shows that

- for $\Delta > 0$ the single real root is positive when $r > -1$ (Domain D), and negative when $r < -1$ (Domain A),
- for $\Delta \leq 0$ we have two positive real roots and one negative real root when $r < -1$ (Domain B and the upper branch of the $\Delta = 0$ curve) and two negative real roots and one positive real root when $r > -1$ (Domain C and the lower branch of the $\Delta = 0$ curve).
- Eq. 27a can serve as a useful check for the calculated values of the roots.

In fact, the roots $\left\{f_{\infty,}^{(1)} f_{\infty,}^{(2)} f_\infty^{(3)}\right\}$ undergo a quite subtle change with the variation of the parameters f_0 and r. This phenomenon is illustrated in Fig. 3 for $-4 < r < +4$ for $f_0 = +3$ and $f_0 = -3$, respectively. In the range $r < -3$ no physical root exists in these cases. For $r = -3$ the discriminant becomes zero, and we get two coincident physical roots (see Table 1),

$$f_\infty = -2\left(\frac{1+r}{2}\right)^{1/3} = 2 \tag{28}$$

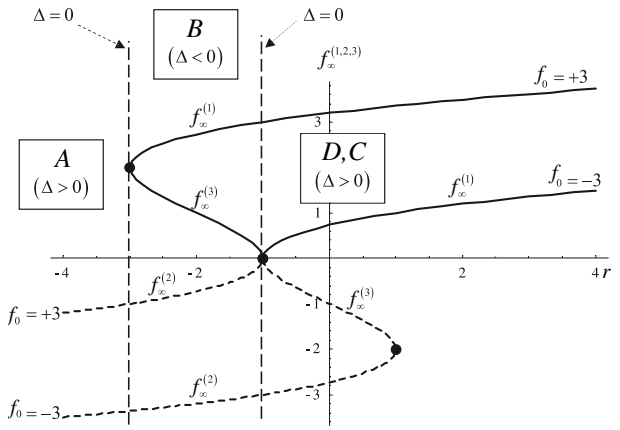

Fig. 3 Trajectories of the roots $\left\{f_{\infty,}^{(1)} f_{\infty,}^{(2)} f_\infty^{(3)}\right\}$ when r varies from -4 to $+4$, for $f_0 = +3$ and $f_0 = -3$, respectively. In the range $-3 \leq r < -1$ the f-boundary value problem admits dual solutions for $f_0 = +3$ which become coincident at $r = -3$. In the range $r > -1$ the solution is unique for $f_0 = +3$. In the case $f_0 = -3$ only unique solutions exist, their domain of existence being $r > -1$. The dashed negative branches are in both cases non-physical

From the solution (20) corresponding to the coincident roots (28), there bifurcate for $r > -3$ two distinct physical solutions (20) of the f-boundary value problem for $f_0 = +3$. With increasing r, the root $f_\infty^{(1)}$ increases, while $f_\infty^{(3)}$ decreases and becomes zero at $r = -1$. For $r > -1$ and $f_0 = +3$ we obtain a single physical root, $f_\infty = f_\infty^{(1)}$, which increases monotonically with increasing r. At $r = 7$, e.g. it reaches the value $f_\infty^{(1)} = 4$. In the case $f_0 = -3$, according to Eq. 26, the coincident roots correspond to $r = +1$ and are non-physical. The physical solutions correspond in this case to the branch $f_\infty^{(1)}$ and are unique. Their domain of existence extends to $r > -1$. The dashed negative branches are in both cases non-physical.

Obviously, the trajectories of the roots $\left\{f_{\infty,}^{(1)} f_{\infty,}^{(2)} f_\infty^{(3)}\right\}$ shown in Fig. 3 also lead to certain trajectories of the similar surface velocity $f'(0)$ given by Eq. 22. This correlation is illustrated in Fig. 4 where the trajectories of the similar interface velocities $\left\{f'^{(1)}(0), f'^{(2)}(0), f'^{(3)}(0)\right\}$ associated with the roots $\left\{f_{\infty,}^{(1)} f_{\infty,}^{(2)} f_\infty^{(3)}\right\}$ are plotted for $f_0 = +3$ and $-4 < r < +2$. The surface velocities are physical in the ranges where the corresponding roots are positive (compare Fig. 4 to Fig. 3).

4 Exact solutions of the temperature problem

The temperature boundary value problem is specified by equation

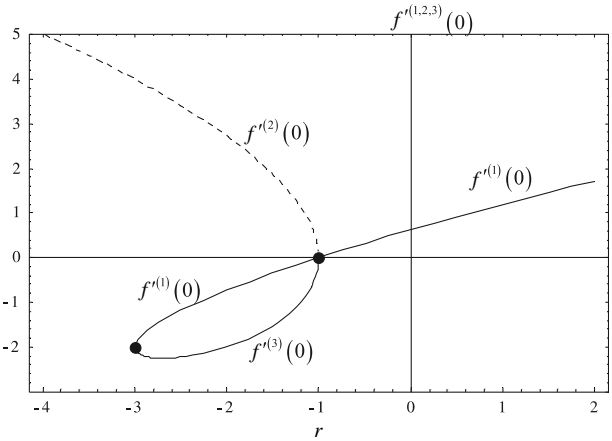

Fig. 4 Trajectories of the similar interface velocities $\left\{f'^{(1)}(0), f'^{(2)}(0), f'^{(3)}(0)\right\}$ associated with the roots $\left\{f_{\infty,}^{(1)} f_{\infty,}^{(2)} f_\infty^{(3)}\right\}$ shown in Fig. 2, as being plotted for $f_0 = 3$ and $-4 < r < +2$. In the range $r < -3$ no physical solutions $f'^{(i)}(0)$ exist. In the range $-3 < r < -1$ we obtain two physical velocities, $f'^{(1)}(0)$ and $f'^{(3)}(0)$, both being negative, and a non-physical solution $f'^{(2)}(0)$ (dashed). For $r > -1$ a single physical solution exists, $f'^{(1)}(0)$, which is positive

$$\frac{\theta''}{Pr} + f\theta' - 2f'\theta + \phi\theta = 0 \tag{29}$$

and the boundary conditions

$$\theta(0) = 1, \tag{30a}$$

$$\theta(\infty) = 0 \tag{30b}$$

Here $f = f(\eta)$ is given by Eq. 20 with $f_\infty \neq f_0$ being a positive root of the cubic equation 21. By the change of variables

$$\theta(\eta) = z^b w(z), \tag{31a}$$

$$z = z_0 e^{-f_\infty \eta}, \tag{31b}$$

$$z_0 = \left(\frac{f_0}{f_\infty} - 1\right) \cdot Pr \tag{31c}$$

equation 29 with $f = f(\eta)$ is given by Eq. 20 goes over in

$$z\frac{d^2w}{dz^2} + (1 + 2b - Pr - z)\frac{dw}{dz} - (b - 2)w = 0 \tag{32}$$

where the constant b satisfies the quadratic equation

$$b^2 - Prb + \frac{\phi Pr}{f_\infty^2} = 0 \tag{33}$$

For a specified value of b Eq. 32 admits two linearly independent solutions

$$\begin{aligned} w_1(z) &= M(b - 2, 1 + 2b - Pr, z), \\ w_2(z) &= z^{Pr-2b} M(Pr - 2 - b, 1 - 2b + Pr, z) \end{aligned} \tag{34}$$

where M denotes Kummer's confluent hypergeometric function M (see [23, Chapt.13]). According to Eq. 31a, the corresponding linearly independent solutions of Eq. 29 are

$$\begin{aligned} \theta_1(\eta) &= e^{-bf_\infty \eta} M(b - 2, 1 + 2b - Pr, z), \\ \theta_2(\eta) &= e^{-(bPr-b)f_\infty \eta} M(Pr - 2 - b, 1 - 2b + Pr, z) \end{aligned} \tag{35}$$

Having in mind that the roots

$$b_{1,2} = \frac{Pr}{2}\left[1 \pm \sqrt{1 - \frac{4\phi}{Prf_\infty^2}}\right] \tag{36}$$

of the quadratic equation 33 satisfy the relationship $b_1 + b_2 = Pr$, it is easy to show that the fundamental solutions 35 of Eq. 29 can be transcribed in the form

$$\theta_{1,2}(\eta) = C_{1,2} e^{-b_{1,2} f_\infty \eta} M\left(b_{1,2} - 2, 1 - Pr + 2b_{1,2}, z\right) \tag{37}$$

where C_1 and C_2 are constants. When both b_1 and b_2 are real and positive, the asymptotic conditions $\theta'_{1,2}(\infty) = 0$ are satisfied automatically and θ_1 and θ_2 yield two independent solutions of the temperature boundary value problem specified by Eqs. 29 and 30. The condition for $b_{1,2} > 0$ requires

$$0 < \frac{4\phi}{Prf_\infty^2} < 1 \quad (b_{1,2} > 0) \tag{38}$$

The constants C_1 and C_2 can be determined in this case from the surface condition (30a) easily. In this way we obtain

$$\theta_{1,2}(\eta) = e^{-f_\infty b_{1,2} \eta} \frac{M\left(b_{1,2} - 2, 1 - Pr + 2b_{1,2}, z\right)}{M\left(b_{1,2} - 2, 1 - Pr + 2b_{1,2}, z_0\right)} \tag{39}$$

The corresponding interface temperature gradients are

$$\theta'_{1,2}(0) = -f_\infty b_{1,2} - f_\infty z_0 \frac{b_{1,2} - 2}{1 - Pr + 2b_{1,2}} \frac{M\left(b_{1,2} - 1, 2 - Pr + 2b_{1,2}, z_0\right)}{M\left(b_{1,2} - 2, 1 - Pr + 2b_{1,2}, z_0\right)} \tag{40}$$

When $\phi < 0$ (heat consumption), b_1 is still real and positive, but b_2 becomes negative. In this case the temperature problem admits a single solution which is θ_1.

We see that for a given solution 20 of the flow boundary value problem, the temperature solutions 39 depend on the heat generation/consumption parameter ϕ and the Prandtl number Pr. As an illustration, in Fig. 5 the temperature profiles (39) corresponding to the parameter values $f_0 = +3$, $r = -2$, $Pr = 3$ and $\phi = 0.3$ are shown. To the corresponding physical roots $f_\infty^{(3)} = 1$ and $f_\infty^{(1)} = 1 + \sqrt{3}$ of the cubic equation 21 there correspond each two temperature profiles θ_1 and θ_2, respectively (the third root of Eq. 21, $f_\infty^{(2)} = 1 - \sqrt{3}$, is negative and thus non-physical; see also Fig. 3). In Table 2 the interface temperature gradients $\theta'_{1,2}(0)$ and the 1%-thicknesses of the temperature profiles plotted in Fig. 5 have been included. The interface temperature gradient specifies the slope of the temperature profile at the interface and the 1% thickness is the value of η for which $\theta = 0.01$. As expected, the temperature boundary layer of the smallest thickness (this is $\theta_1(\eta)$ for $f_\infty^{(1)} = 1 + \sqrt{3}$, with $\eta_1 = 0.569606$) leads to the largest interface heat transfer ($\theta'_1(0) = -8.290731$) and that of the largest thickness (this is $\theta_2(\eta)$ for $f_\infty^{(1)} = 1 + \sqrt{3}$, with $\eta_2 = 38.6795$) leads to the smallest interface heat transfer ($\theta'_2(0) = -0.921958$).

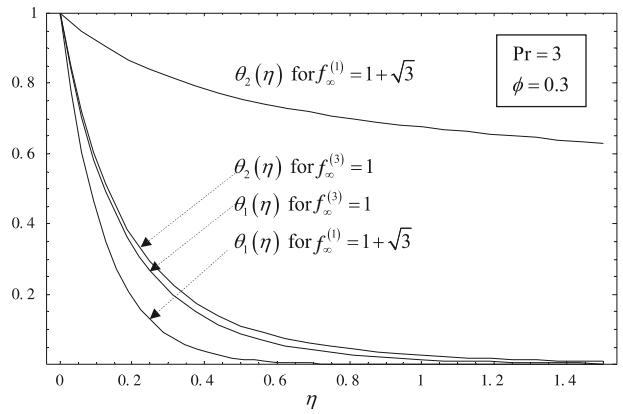

Fig. 5 Temperature profiles (39) corresponding to the parameter values $f_0 = 3$, $r = -2$, $Pr = 3$ and $\phi = 0.3$. Each two profiles (with the same values of $Pr = 3$ and $\phi = 0.3$) correspond to the roots $f^{(3)}{}_\infty = 1$ and $f_\infty^{(1)} = 1+\sqrt{3}$ of the cubic equation 21, respectively (see also Fig. 3)

When some special relationships between the parameters ϕ and Pr hold, the solutions 39 can be reduced to simpler (even elementary) forms. In the following we consider such special cases, namely the cases for which $b_1 = 2$. One immediately sees that the special case $b_1 = 2$ can be realized for the values

$$\phi = \frac{2(Pr-2)}{Pr} f_\infty^2 \tag{41}$$

of the heat generation/consumption parameter ϕ. The salient aspect of this case is that the corresponding solution $\theta_1(\eta)$ becomes especially simple,

$$\theta_1(\eta) = \mathrm{e}^{-2f_\infty \eta},\ \theta'_1(0) = -2f_\infty, (b_1 = 2) \tag{42}$$

The second solution, $\theta_2(\eta)$ (associated with the same values of f_0, f_∞, ϕ and Pr), is also a physical solution when $b_2 = Pr - 2 > 0$, i.e. when $Pr > 2$, which according to Eq. 41 requires $\phi > 0$. For $Pr \le 2$, i.e. for $\phi \le 0$ the second solution associated with (42) is non-physical. As an illustration of the cases $b_1 = 2$, the dependence of ϕ, as given by Eq. 41, on the parameter r is plotted in Figs. 6 and 7 for $f_0 = +3$ and $Pr = 1$ and $Pr = 6$, respectively. In the latter case, $Pr = 6$, the temperature problem admits in addition to 42 a second solution, $\theta_2(\eta)$ given by Eq. 39 with $b_1 = 2$ and $b_2 = Pr - b_1 = 4$,

$$\theta_2(\eta) = \mathrm{e}^{-4f_\infty \eta} \frac{M(2,3,z)}{M(2,3,z_0)} \tag{43a}$$

In this case the Kummer functions M in Eq. 43a can also be expressed by elementary functions yielding

$$\theta_2(\eta) = \mathrm{e}^{-2f_\infty \eta} \frac{1-(1-z)\mathrm{e}^z}{1-(1-z_0)\mathrm{e}^{z_0}} \tag{43b}$$

where z is given by Eqs. 31b,c.

Table 2 The values of the interface temperature gradients $\theta'_{1,2}(0)$ and of the 1%-thicknesses of the temperature profiles plotted in Fig. 5 ($f_0 = +3$, $r = -2$, $Pr = 3$ and $\phi = 0.3$)

	$-\theta'_1(0)$	$-\theta'_2(0)$	1% thickness	
			η_1	η_2
$f^{(3)}{}_\infty = 1$	5.90091	5.608182	1.107181	1.44577
$f_\infty^{(1)} = 1+\sqrt{3}$	8.290731	0.921958	0.562415	38.6795

5 Exact solutions of the concentration problem

The concentration boundary value problem is specified by equation

$$\frac{C''}{Sc} + fC' - 2f'C - K\theta = 0 \tag{44}$$

and the boundary conditions

$$C(0) = 1, \tag{45a}$$

$$C(\infty) = 0 \tag{45b}$$

Comparing Eqs. 44 and 45 to Eqs. 29 and 30, we see that the solutions of the concentration problem can formally be gained from those of the temperature problem by simply replacing θ by C, Pr by Sc and ϕ by $-K$, respectively. Nevertheless, there occurs an essential difference which is due to the fact that, in contrast to ϕ,

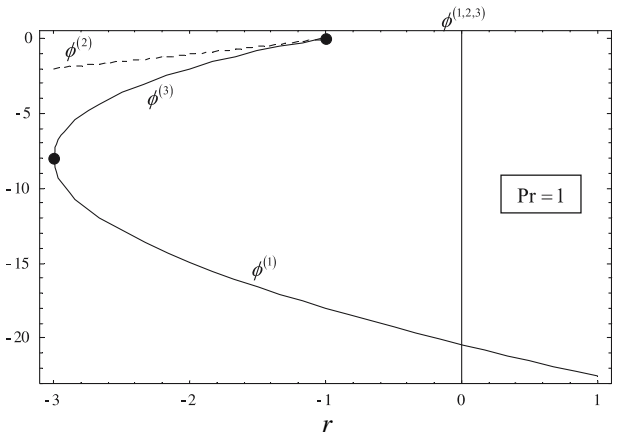

Fig. 6 Trajectories of $\phi^{(1,2,3)}$ associated according to Eq. 41 with the roots $\left\{f_{\infty,}^{(1)} f_\infty^{(2)} f_\infty^{(3)}\right\}$ shown in Fig. 3, as being plotted for $f_0 = +3$, $-3 < r < +1$ and $Pr = 1$. For the corresponding values of $\phi^{(1,2,3)}$ the temperature solution is given by Eq. 42. The branch $\phi^{(2)}$ (dashed) is non-physical

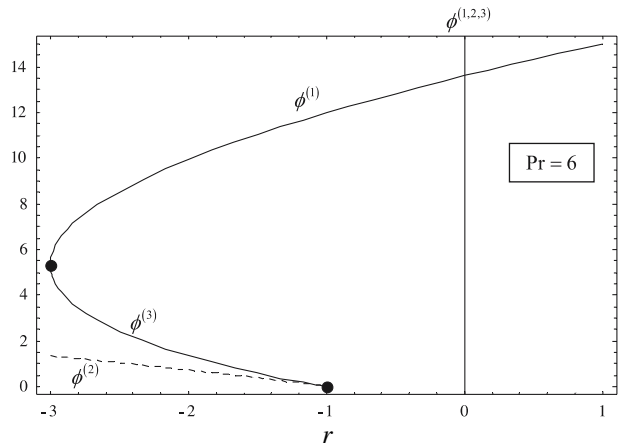

Fig. 7 Trajectories of $\phi^{(1,2,3)}$ associated according to Eq. 41 with the roots $\left\{f_{\infty}^{(1)} f_{\infty}^{(2)} f_{\infty}^{(3)}\right\}$ shown in Fig. 2, as being plotted for $f_0 = +3, -3 < r < +1$ and $Pr = 6$. For the corresponding values of $\phi^{(1,2,3)}$ the temperature problem admits two independent solutions, $\theta_1(\eta)$ given by Eq. 42, and $\theta_2(\eta)$ given by Eq. 43. The branch $\phi^{(2)}$ (dashed) is non-physical

the reaction parameter$K$ given by the second Eq. 13 is strictly positive and thus the transcribed Eqs. 36,

$$b_{1,2} = \frac{Sc}{2}\left[1 \pm \sqrt{1 + \frac{4K}{Scf_{\infty}^2}}\right] \tag{46}$$

always yield one negative root, b_2, such that the corresponding solution $C_2(\eta)$ obtained by transcription of $\theta_2(\eta)$ violates the asymptotic condition $C(\infty) = 0$. As a consequence, the concentration problem always admits a unique solution, namely the counterpart of $\theta_1(\eta)$. In this way the subscript 1 may be omitted, and the concentration solution [obtained from Eq. 39] reads

$$C(\eta) = \mathrm{e}^{-f_{\infty} b\,\eta} \frac{M(b-2, 1-Sc+2b, z)}{M(b-2, 1-Sc+2b, z_0)} \tag{47}$$

Here $b \equiv b_1$ (as being given by Eq. 46 with sign +) and, according to Eq. 31c,

$$z_0 = \left(\frac{f_0}{f_{\infty}} - 1\right) \cdot Sc \tag{48}$$

The corresponding interface concentration gradient (as being obtained from Eq. 40 is

$$C'(0) = -f_{\infty} b - f_{\infty} z_0 \frac{b-2}{1-Sc+2b_{1,2}} \frac{M(b-1,2-Sc+2b, z_0)}{M(b-2,1-Sc+2b, z_0)} \tag{49}$$

We note that for small values of the Schmidt number the interface concentration gradient (49) scales with Sc as

$$C'(0) = -\sqrt{K \cdot Sc}\,(Sc \ll 1) \tag{50}$$

For $b = 2$ Eqs. 47 and 49 reduce to

$$C(\eta) = \mathrm{e}^{-2f_{\infty}\eta},\ C(0) = -2f_{\infty}\,(b_1 = 2) \tag{51}$$

which are counterparts of Eqs. 42. Similarly to Eq. 41, $b = 2$ can be realized in this case for the values

$$K = \frac{2(2-Sc)}{Sc} f_{\infty}^2 \tag{52}$$

of the reaction parameter K.

6 Summary and conclusions

Exact analytical solutions for the velocity, temperature and concentration fields of steady thermosolutal Marangoni in the presence of temperature-dependent volumetric heat sources/sinks as well as of a first-order chemical reaction have been reported in this paper. The dependence of the solutions on the parameters f_0 (normal component of the dimensionless interface velocity), r (ratio of the solutal and thermal Marangoni numbers), ϕ (dimensionless heat generation/absorption coefficient), K (dimensionless chemical reaction coefficient), Prandtl number Pr and Schmidt number Sc has been examined in some detail. The main results of the paper can be summarized as follows:

1. The flow solutions depend only on the parameters r and f_0. Their domain of existence in the parameter plane (r,f_0) is shown in Table 1 and Fig. 2.
2. Depending on the values of r and f_0 there may exist either unique or dual flow solutions (see Fig. 3) associated with one of two different positive values of the similar entrainment velocity f_{∞} (see Fig. 3).
3. The similar interface velocities $f'(0)$ are quadratic functions of the entrainment velocities f_{∞} [see Eq. 22] and depend on r and f_0 via f_{∞} sensitively (see Fig. 4).
4. For a given solution of the flow problem and specified values of ϕ and Pr, the temperature problem admits in general one or two linearly independent solutions which can be expressed in term of Kummer's confluent hypergeometric functions. The characteristics of these solutions has been discussed in Sect. 5 in detail (see also Fig. 5 and Table 2). The interface heat transfer coefficient could also be calculated exactly [see Eqs. 40].
5. When between the parameters ϕ and Pr a special relationships holds [see Eq. 41], the general temperature solutions can be reduced to some

elementary forms [see Eqs. 42 and 43, and Figs. 6 and 7]. One of these solutions is always a simple exponential function [see Eq. 42]. Thus Eq. 41 represents precisely the condition under which the approximate solutions reported recently by Al-Mudhaf and Chamkha [21] become exact.

6. With some precaution, the solutions of the concentration boundary value problem can be obtained by a simple transcription of the temperature solutions (see Sect. 5).

References

1. Napolitano LG (1978) Microgravity fluid dynamics, In: 2nd Levitch Conference, Washington, 1978
2. Napolitano LG (1979) Marangoni boundary layers, In: Proceedings of the 3rd European symposium on material science in Space, Grenoble, ESA SP-142, June 1979
3. Christopher DM, Wang B (2001) Prandtl number effects for Marangoni convection over a flat surface. Int J Therm Sci 40:564–570
4. Eyer A, Leist H, Nitsche R (1985) Floating zone growth of silicon under microgravity in sounding rocket. J Crystal Growth 71:173–182
5. Straub J (1994) The role of surface tension for two phase heat and mass transfer in the absence of gravity. Experiment Therm Fluid Sci 9:253–273
6. Napolitano LG (1982) Surface and buoyancy driven free convection. Acta Astronautica 9:199–215
7. Napolitano LG, Golia C (1981) Coupled Marangoni boundary layers. Acta Astronautica 8:417–434
8. Napolitano LG, Russo G (1984) Similar axially symmetric Marangoni boundary layers. Acta Astronautica 11:189–198
9. Golia C, Viviani A (1985) Marangoni buoyant boundary layers. L'Aerotechnica Missili e Spazio 64:29–35
10. Golia C, Viviani A (1986) Non isobaric boundary layers related to Marangoni flows. Meccanica 21:200–204
11. Napolitano LG, Carlomagno GM, Vigo P (1977) New classes of similar solutions for laminar free convection problems. Int J Heat Mass Transfer 20:215–226
12. Pop I, Postelnicu A, Groşan T (2001) Thermosolutal Marangoni forced convection boundary layers. Meccanica 36:555–571
13. Arafune K, Hirarta A (1998) Interactive solutal and thermal Marangoni convection in a rectangular open boat. Numer Heat Tran Part A 34:421–429
14. Croll A, Muller-Sebert W, Nitsche R (1989) The critical Marangoni number for the onest of time-dependent convection in silicon. Mater Res Bull 24:995–1004
15. Okano Y, Itoh M, Hirata A (1989) Natural and Marangoni convections in a two-dimensional rectangular open boat. J Chem Engrg Japan 22:275–281
16. Arafune K, Sugiura M, Hirata A (1999) Investigation of thermal Marangoni convection in low and high Prandtl number fluids. J Chem Engrg Japan 32:104–109
17. Arafune K, Hirata A (1999) Thermal and solutal Marangoni convection in In-Ga-Sb system. J Crystal Growth 197:811–817
18. Slavtchev S, Miladinova S (1998) Thermocapillary flow in a liquid layer at minimum in surface tension. Acta Mechanica 127:209–224
19. Schwabe D, Metzger J (1989) Coupling and separation of buoyant and thermocapillary convection. J Crystal Growth 97:23–33
20. Napolitano LG, Viviani A, Savino R (1992) Double-diffusive boundary layers along vertical free surfaces. Int J Heat Mass Transfer 35:1003–1025
21. Al-Mudhaf A, Chamkha A (2005) Similarity solutions for MHD thermosolutal Marangoni convection over a flat surface in the presence of heat generation or absorption effects. Heat Mass Transfer 42:112–121
22. Christopher D, Wang B (1998) Marangoni convection around a bubble in microgravity, heat transfer. In: Lee JS (ed) Proceedings of the 11th international Heat Transfer Conference, Vol. 3, Taylor & Francis, Levittown, pp 486–494
23. Abramowitz M, Stegun IA (1964) Handbook of mathematical functions. Dover, New York